DOI: 10.31577/ahs-2024-0025.01.0013

ACTA HYDROLOGICA SLOVACA

Volume 25, No. 1, 2024, 115 – 126

Evaluating flood events caused by Medicane "Daniel" in the Thessaly District (Central Greece) using remote sensing data and techniques

Evangelos LEIVADIOTIS*, Silvia KOHNOVÁ, Aris PSILOVIKOS

On September 4, 2023, Thessaly, Greece, underwent a catastrophic flood due to Medicane Daniel. Extreme rainfall, ranging from 305 mm to 1096 mm between 4 and 12 September, caused extensive damage to the infrastructure, agriculture and houses. Seventeen casualties were recorded. This study is aimed at using radar data from earth observation satellites to detect the inundated areas and evaluate the impact of the flood. Sentinel images were acquired from Copernicus Open Acess Hub For 7, 10, 13, and 19 September, 2023, along with a CORINE Land use/Land cover map. Processing the satellite images involved several steps, including their calibration, noise removal, filtering, and polarization adjustments. Flooded areas were quantified for the specified dates, thereby revealing substantial coverage of the land. The damage assessment focused on irrigated and non-irrigated land and pasture areas, highlighting the impact's severity. The highest impact was noticed on September 7 in irrigated land (95.62%). The second phase incorporated the Flood Water Depth Estimation Tool (FwDET) to estimate the floodwater depths and reveal the maximum depths near riverbanks. The maximum floodwater depth was also noticed on September 7 and reached 9.49 m. This study employed advanced remote sensing and GIS techniques, allowing for a rapid estimation of flood characteristics and assessment of Medicine Daniel's damage to the Thessaly prefecture from September 4 to 12, 2023.

KEY WORDS: flood, Medicane Daniel, Thessaly, remote sensing, damage assessment, Sentinel-1

Introduction

Flooding is a natural process that greatly impacts a drainage basin's hydrology. However, with regard to human activity, floods are regarded as a type of natural disaster (Pekárová et al., 2003). In reality, especially in the countries of the Mediterranean, floods are among the most frequent, expensive, and destructive catastrophic events (Thomas et al., 2023; Jorkman et al., 2005; Khajehei et al., 2020). For local and regional communities, they represent a serious economic threat (Kellermann et al., 2015). The primary causes of this threat are the numerous small catchments and the frequent occurrence of rain events involving heavy and rapid precipitation. In Mediterranean regions, flash floods are the most frequent type of flooding due to small river basins with short flow concentration times, high slopes or low permeability of the soil and geological formations and, most importantly, heavy precipitation (Diakakis et al., 2012). Greece is more vulnerable to flooding than the majority of European nations because of its numerous small, mountainous catchments and large floodplains, i.e., its Mediterranean climate, which frequently experience extreme weather events; its lithological structure, which contains numerous impermeable lithologies; its sparse forest cover, and countless human interventions (Diakakis et al., 2012). It is considered one of the European nations that experiences the greatest number of floods with the worst damage from them, which have rapidly increased over the past few decades (Diakakis et al., 2022; Diakakis et al., 2011). It is noteworthy that flash floods account for most Greek floods, despite many efforts to prevent them. At this point, in time, however, recordings and data on floods are scarce.

Remote sensing (RS) techniques, particularly satellite imagery, provide a valuable source of information for mapping flooded surfaces with sufficient temporal and geographical resolutions; they offer accurate and continuous data to aid in disaster mitigation, especially for floods (Hrušková and Hlaváčiková, 2023). These observations cover vast and inaccessible areas, enabling the identification of bodies of water over extensive distances and facilitating crucial information for risk and damage assessments (Buta et al., 2020; Bioresita et al., 2019; Craciunescu et al., 2016; Psomiadis, 2016; Klemas, 2015). Sentinel-1 Synthertic Aperture Radar (SAR) images has been increasingly widespread for flood extent mapping in flood hazard studies as they provide accurate and high resolution results (Huang and

Jin, 2020; Uddin et al., 2019)

The Copernicus program of the European Space Agency (ESA) provides precise, timely, and freely accessible Synthetic Aperture Radar (SAR) data of the Sentinel-1 satellite system. It can function day and night, is unaffected by atmospheric water, smoke, and clouds, and offers comprehensive details regarding the state of an inundation. Every ten days, Sentinel-2 (S2), a brand-new land monitoring and classification satellite, produces optical spatial resolution imagery for terrestrial observations covering the whole planet's land surface. Its data are highly beneficial for mapping land use and cover and quantifying associated changes.

Road closures, accessibility, and the allocation of emergency and humanitarian resources depend on timely information regarding floodwater depths. Whenever accessible, flood depth or peak flow data can also be utilized for flood-risk assessments and post-event studies of property damage (Výleta et al., 2023; Islam et al., 2001; Nadal et al., 2010). Various methods have been developed for estimating floodwater depths using flood maps derived from remote sensing (Šoltész et al., 2011; Nguyen et al., 2016; Schumann et al., 2010). Cohen et al. (2018) employed a concept akin to cross sections in their Floodwater Depth Estimation Tool (FwDET). Unlike, ordinary cross sections, FwDET determines floodwater elevations for each cell within a flooded domain by referencing the nearest flood-boundary grid cell, thereby eliminating any requirement for specific data. This approach maintains usability with complex and fragmented flood extent maps from any source and resolution, making it sensor and platform-independent.

In early September 2023, Europe experienced severe weather conditions due to an Omega block, which is characterized by a high-pressure system between two low-pressure systems. This atmospheric pattern persisted for over a week. Storm Daniel, which was linked to this setup, caused catastrophic flooding in central and eastern Greece, including Thessaly prefecture, which was triggered by warm, moist air colliding with cold upper air. Storm Daniel originated in Greece, was named by the Hellenic National Meteorological Service, and significantly impacted the Mediterranean region. The storm moved inland over the Balkans on September 4, 2023, resulting in intense rainfall and thunderstorms. Central Greece witnessed substantial daily rainfall, leading to at least 15 fatalities and unprecedented flooding.

This research aims at presenting and evaluating a new approach that uses only the extent of the flood data acquired by Sentinel imagery and a digital elevation model (DEM) to estimating the depths of the water in the flooded domains caused by Storm Daniel. The first part of the study maps the inundated areas using SAR images and assesses the land use/land cover damage. The other part focuses on estimating floodwater depths using the Floodwater Depth Estimation Tool (FwDET), a straightforward Python script used in the methodology to combine common geographic information system (GIS) capabilities. Due to its relative simplicity, FwDET can rapidly calculate floodwater depth rapidly with easily accessible data, which is a handy feature for near-real-time flood mapping applications or systems that evaluate several floods.

Material and methods

Study area

The study area resides in the Pinios River basin (GR16), the largest catchment in the Thessaly Water District (GR08); it has an area of 10,700 km^2, a mean annual rainfall of 779 mm, and a mean annual runoff of 3500 m^3 s^{-1} (327 mm). It is situated between 39°11' N and 39°58' N latitude and 21°52' E and 22°45' E longitude (Fig. 1). It is bordered by an extensive plain and several mountainous areas, notably Olympus, the highest mountain in Greece (2918 m). The most fertile and productive agricultural lands in Greece can be found on the Thessaly Plain, which is located in the catchment's centre and mainly consists of a flat terrain subsequently covered with alluvial deposits (Orengo et al., 2015). In particular, agriculture constitutes 49.5% of the Thessaly Water District's land area, while the Thessalian Plain is estimated to represent the production site for 14.2% of Greece's primary products (YPEKA, 2018). The Pindus Sierra, Greece's most extensive mountain range, is the source of the Pinios River, which discharges into the Aegean Sea.

The Pinios River Basin's geomorphological features, such as its circular catchment and its gradually sloping terrain, favour inundation conditions and make it more vulnerable to flood disasters. In particular, a number of historically significant floods, including those that occurred on June 4, 1907, October 27, 1980, March 23, 1987, and October 22, 1994, have been documented, according to the EU Floods Directive (2007/60/EC)-Preliminary Flood Risk Assessment, which was implemented by the Ministry of the Environment and Energy of Greece. Additionally, 31.7% of the total area of the Thessaly Water District is classified as an area of potentially significant flood risks (YPEKA, 2018).

Data

The materials and methodology employed to fulfil the objectives of this study can be categorized into two main sections. The initial section encompasses inundation mapping utilizing SAR images, while the subsequent section focuses on calculating flood depths using the FwDET tool and damage assessment. SNAP software was used for pre-processing Sentinel images, including calibration, noise removal, a speckle filter, and the terrain correction. A Corine Land use/Land cover map (2018) (https://land.copernicus.eu/en/products/corine-land-cover), and ALOS PALSAR DEM (https://asf.alaska. edu/) (10m resolution) were used to assess the flood damage and calculate the depth of the water, respectively. The Sentinel-1 and Sentinel-2 cloud free images were downloaded via the Copernicus Open Access Hub platform (https://sentinel.esa.int/web/sentinel/home; ESA, 2019) during the catastrophic event. Each image has a coverage range of 250 km with a 5 × 20 m resolution (Table 1). The images are Level-1

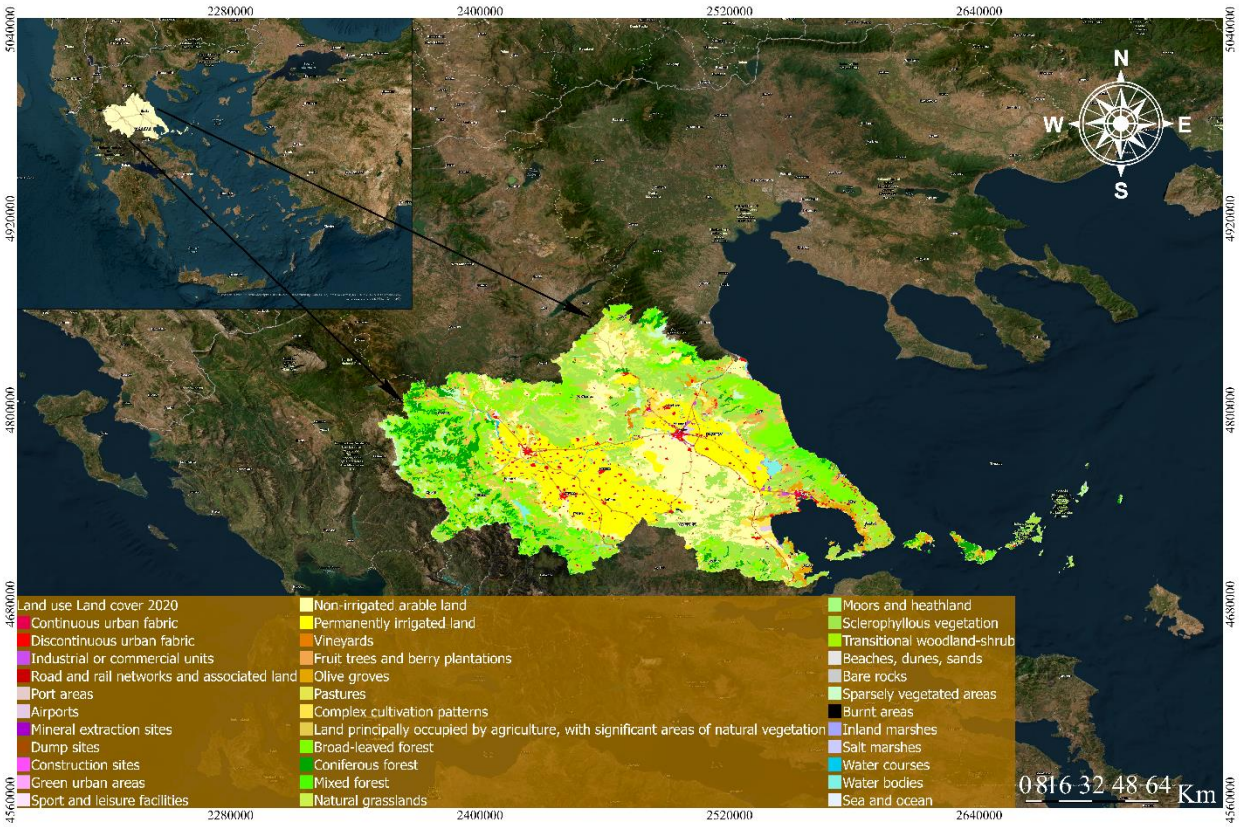

Fig. 1. Land use / Land cover map of Thessaly district (Greece).

Table 1. Characteristics of the Sentinel images used in the study

Satellite	Instrument	Image Code	Acquisition Date	Pixel resolution	Path	Frame	Flight Direction
Sentinel-1	C-SAR	S1A_IW_GRDH_1SDV_20230907T 162437_20230907T162502_050224_ 060B99_3635	07/09	10m	102	128	Ascending
Sentinel-1	C-SAR	S1A_IW_GRDH_1SDV_20230907T 162412_20230907T162437_050224_ 060B99_D80F	07/09	10m	102	123	Ascending
Sentinel-2	MSI	S2B_MSIL2A_20230910T091559_N 0509_R093_T34SEJ_20230910T131 613.SAFE	10/09	10m	-	-	Descending
Sentien-2	MSI	S2B_MSIL1C_20230910T091559_N 0509_R093_T34SFJ_20230910T1153 23.SAFE	10/09	10m	-	-	Descending
Sentinel-2	MSI	S2B_MSIL2A_20230910T091559_N 0509_R093_T34TFK_20230910T121 340.SAFE	10/09	10m	-	-	Descending
Sentinel-1	C-SAR	S1A_IW_GRDH_1SDV_20230913T 043132_20230913T043157_050304_ 060E62_436A	13/09	10m	7	458	Descending
Sentinel-1	C-SAR	S1A_IW_GRDH_1SDV_20230913T 043157_20230913T043222_050304_ 060E62_258F	13/09	10m	7	463	Descending
Sentinel-1	C-SAR	S1A_IW_GRDH_1SDV_20230919T 162437_20230919T162502_050399_ 061199_CF8F	19/09	10m	102	128	Ascending
Sentineal-1	C-SAR	S1A_IW_GRDH_1SDV_20230919T 162412_20230919T162437_050399_ 061199_0F25	19/09	10m	102	123	Ascending

Ground Range Detected (GRD) products; they were detected, viewed multiple times, and projected to the ground range using an Earth ellipsoid mode. The acquisition mode was Interferometric Wide Swath, and the images have a high resolution; the sensor pass is ascending, with dual polarization, VV (Vertical-Vertical) and VH (Vertical-Horizontal). SNAP software was used for the digital image processing and satellite data analysis, while ArcGIS was used for the spatial data processing.

Sentinel pre-processing steps

We performed a series of seven pre-processing steps using SNAP software to get the final inundation maps. The first step was to apply an orbit file, which automatically downloads and updates the orbit state vectors in its product metadata for each SAR scene, thereby providing accurate satellite positions and speed information. Then, the thermal noise removal normalizes the backscatter signal in each scene, which reduces any discontinuities for multi-swath acquisition models between the sub-swarths. Applying the border noise removal next removes low-intensity noise and invalid data on the edges of the scene. Subsequently, calibration, a process in which pixel values are converted to radiometrically calibrated SAR backscatter, is performed. One feature of the images captured by SAR instruments is the random noise, or "speckling," which appears within the image and resembles a "salt and pepper" effect. In order to mitigate this effect, speckle filtering, a process that reduces the effect of speckling and enhances the image quality, is applied. This study used a Lee filter (7X7 window) among the various filters. The Range Doppler Terrain Correction operator applies the Range Doppler ortho-rectification algorithm. To bring the image's geometric representation as close to reality as possible, terrain adjustments compensated for these distortions. The Sentinel-1 SAR image pre-processing finishes by converting the image to decibel scaling, which, the SNAP software can handle automatically and the final sigma dB was used using backscattering values below -20 dB (Fig. 2). Sentinel-2 image processing steps included mosaic raster, RGB combinations to distinguish the flooded area followed by pixel sampling and applying the maximum likelihood classification (MLC) algorithm to detect the inundated areas (Aziz and Alwan, 2021). The validation of inundated areas Fig. 3 shows that the workflow applied is used to derive the flood inundation maps of each time frame and contains the classification of pixels into water and non-water bodies. The calibration threshold technique, also known as binarization, is the most widely accepted method and distinguishes flooded areas from non-flooded ones through histogram generation, with two methods employed for preprocessing SAR images:

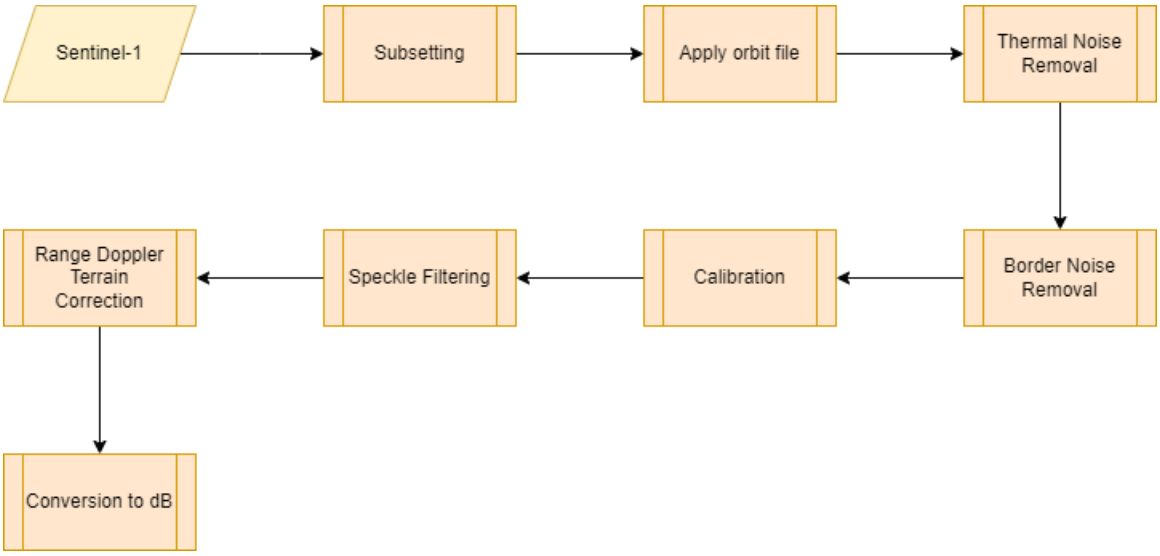

Fig. 2. Pre-processing steps of Sentinel-1 images.

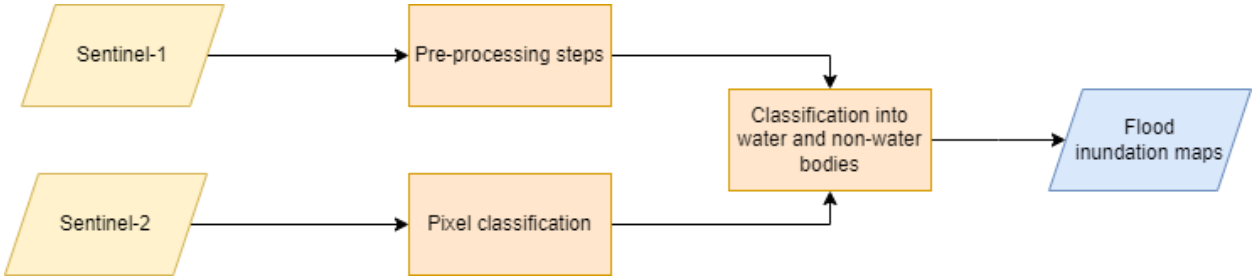

Fig. 3. Workflow deriving flood inundation maps from Sentinel images.

binarization utilizing dual threshold values for water area detection, and image differencing between pre- and during-event images to enhance them for subsequent analysis. Validation process is essential for every product of satellite image in order to enhance the use of remote sensing data and techniques. In this study, kappa coefficient was used as it is one of the most popular metrics when it comes to classification methods. The Copernicus delineation monitoring products were used as reference data derived from https://rapidmapping.emergency.copernicus.eu/ and compared with the images of September 7 and 10, 2023 as they were the most recent and closed to date with Copernicus product (September 7 and 9, 2023). Products for the rest of the dates were not available due to the termination of the event. Accuracy assessment according to kappa coefficient results were excellent as for 7 of September reached an accuracy of 78.95% and for 10 of September, 80%, providing satisfying results for proceeding in the following steps. However, the need of ground truth data and additional supportive material of other agencies from different dates of the event will improve this research.

The implementation of the FwDET tool

Cohen et al. (2018) described in detail the fundamental methodology for calculating the floodwater depth using the FwDET tool. Step 1 in the implementation of the FwDET tool involves converting a flood inundation polygon into a polyline layer, then transforming it into a raster layer with specified cell dimensions. This raster layer assigns "No Data" values to non-relevant cells and identifies boundary cells, even for complex floods, resulting in a raster representation of the flooded area. Using ArcGIS Map Algebra, a new raster layer is created by applying conditional raster calculations where boundary cells from Step 1, excluding "No Data" cells, are assigned elevation values from the DEM. The "Focal Statistics" tool is then used to generate another raster layer, where each cell is iteratively assigned the elevation of its nearest boundary cell by increasing the neighbourhood size in a conditional loop, ensuring all cells receive the elevation of their closest boundary cell, with a circular neighbourhood geometry for smoother results (Step 3). The floodwater depth is calculated by subtracting the DEM value from the raster layer generated in Step 3, representing the elevation of the nearest boundary cell, using an ArcGIS Map Algebra expression and clipping the DEM to include only cells within the flooded area to account for values on both sides of the boundary cells. To mitigate sharp changes in the floodwater depths arising from spatial mismatches or actual transitions, a smoothing procedure is applied using the "Filter" tool with a "low-pass" option in FwDET, which calculates the average value for each cell based on its 3 × 3 neighbourhood.

Results and discussion

Inundated areas

Storm Daniel started on September 4, 2023, and ended on September 9, 2023, causing severe damage across Central Greece. This study proposes a methodology of using Radar Sentinel products for flood monitoring and damage assessment and tools like FwDET for estimating rapid water depths. Fig. 4 represents the inundated areas of September 7, 2023. Through the analysis of the Sentinel images, it was noticed that on the first two

Fig. 4. Map of Thessaly's inundated areas, September 7th.

dates (September 7 and September 10, 2023), the total area covered by water was more than that on the last two dates (September 13 and September 19, 2023). This could be explained by the fact that on the first date (September 7, 2023), the phenomenon was still ongoing. The following image was right after the end of the event (September 10, 2023) (Fig. 5). On September 7, 2023, inundated areas covered 223.34 km^2, with most of the flooded areas in Western Thessaly (Fig. 4.). The following image was acquired on September 10, 2023, right after the end of the storm. It shows the greatest extent of the flooding, which covered 516.52 km^2 and extended from western to eastern Thessaly. After three days, on September 13, 2023, the flooded areas derived from the Sentinel image showed a significant decrease, covering 169.70 km^2; it was primarily located in Eastern Thessaly at Lake Karla (Fig. 6).

Lastly, even after ten days since the end of the phenomenon, the total area covered by water accounted for 109.43 km^2 in that part of Eastern Thessaly (Fig. 7).

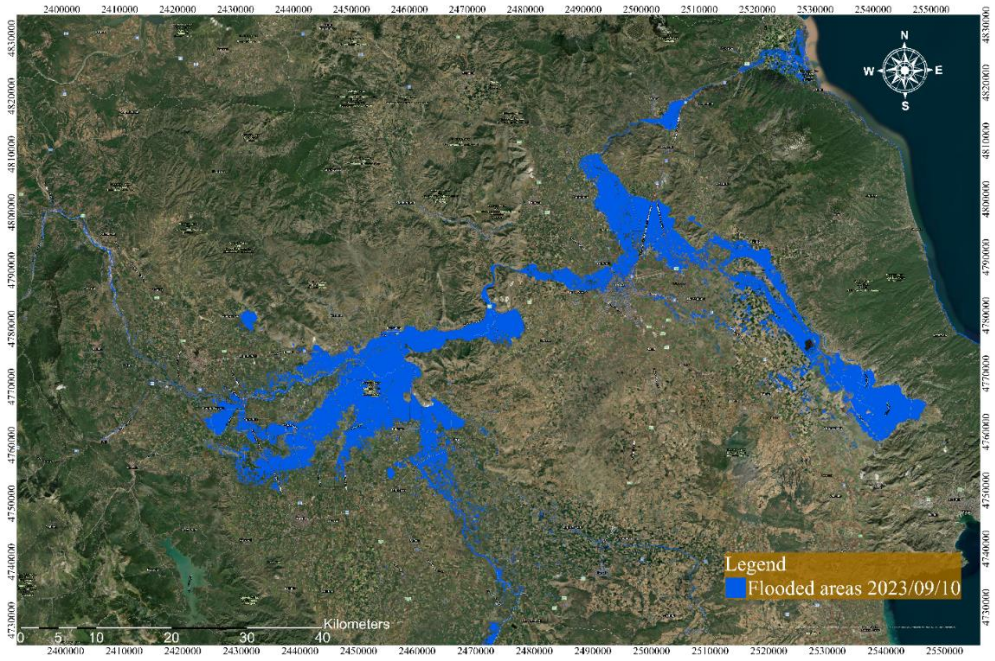

Fig. 5. Map of Thessaly's inundated areas, September 10, 2023.

Fig. 6. Map of Thessaly's inundates areas, September 13, 2023.

Analysis of floodwater depths

The investigation assessed the depth of the inundation at various locations over a specified temporal interval. The initial observations from Fig. 5 delineated a discernible trend in the floodwater depths, indicating an increase from September 7 to 10, 2023, followed by a gradual decline until September 19, 2023. Specifically, on September 7, 2023, the maximum inundation depth reached 9.49 m, with notable concentrations near riverbanks denoted by red circles within the Western Thessaly region (Fig. 8). This pattern persisted on September 10, with expanded flood coverage and heightened depths in multiple areas (Fig. 9). Subsequently, on September 13, 2023, a discernible reduction in the floodwater depths was observed, with the maximum value registering at 7.35 m (Fig. 10). In conclusion, the temporal analysis on September 19, 2023, exhibited a significant and abrupt decrease in the floodwater depths, reaching a minimum of 2.34 m in the vicinity of the Lake Karla region in eastern Thessaly (Fig. 11).

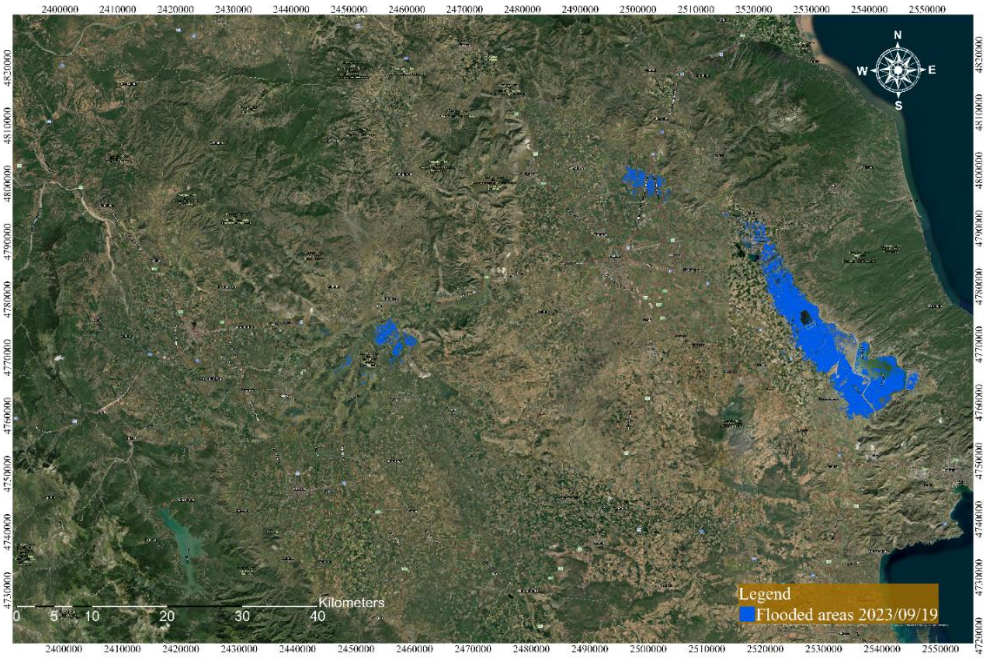

Fig. 7. Map of Thessaly's inundated areas, September 19, 2023.

Fig. 8. Distribution of flood water depths estimated by the FwDET tool (September, 7, 2023, red circles indicate regions of high depth).

Fig. 9. Distribution of flood water depths estimated by the FwDET tool (September, 10, 2023, red circles indicate regions of high depth).

Fig. 10. Distribution of flood water depth estimated from FwDET tool (September, 13, 2023, red circles indicate regions of high depth).

Land use/Land cover damage assessments

The extent of losses and damage caused by floods depends on the duration and extent of the flooding. The other part of our analysis investigated the spatio-temporal effects of flooding in a detailed spatial resolution involving an overlay of the temporally recorded inundation areas onto a classified land cover map provided by Corine. On September 7, 2023, the outcomes revealed that 95.62% of the Land Use and Land Cover (LULC) flooded area primarily comprised irrigated land (Fig. 12). By September 10, 2023, the most significantly affected areas encompassed irrigated land, non-irrigated land, and pasture, constituting 72.81%, 15.57%, and 2.28% of the total area coverage, respectively (Fig. 12). Fig. 12 illustrates the extent of damage to each land use class on September 13, 2023, indicating that irrigated land accounted for 71.30%, water bodies for 18.27%, non-irrigated land for 4.73%, and pasture for 2.34% of the total area cover.

Fig. 11. Distribution of flood water depth estimated from FwDET tool (September, 19, 2023, red circles indicate region of high depth).

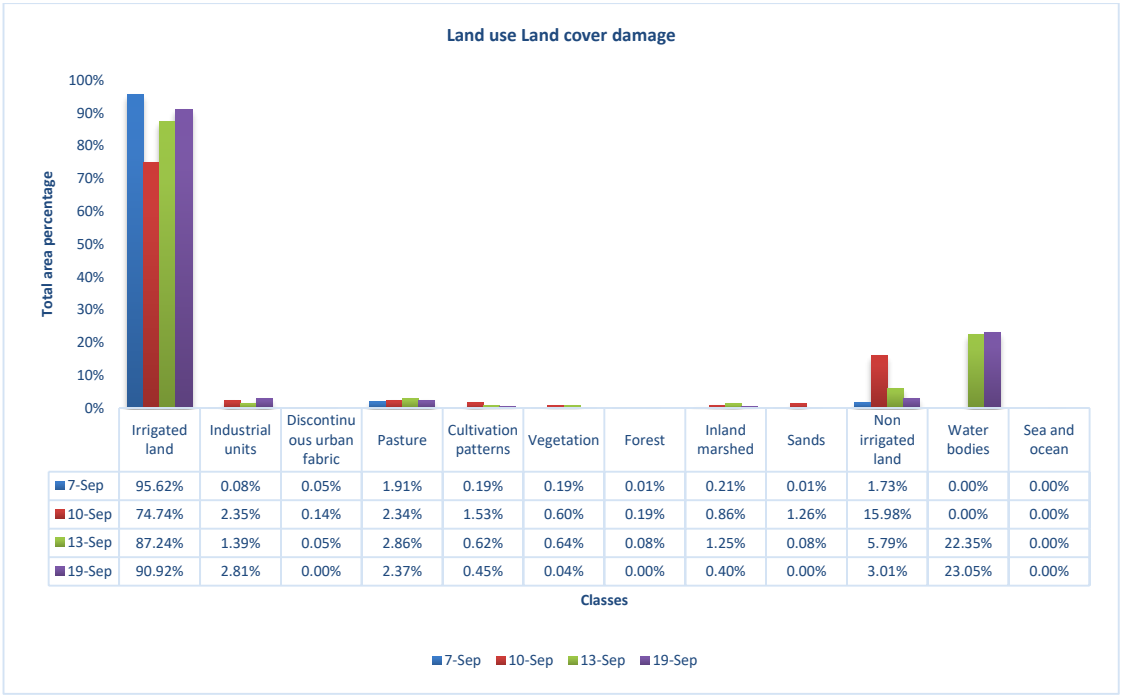

	Irrigated land	Industrial units	Discontinuous urban fabric	Pasture	Cultivation patterns	Vegetation	Forest	Inland marshed	Sands	Non irrigated land	Water bodies	Sea and ocean
7-Sep	95.62%	0.08%	0.05%	1.91%	0.19%	0.19%	0.01%	0.21%	0.01%	1.73%	0.00%	0.00%
10-Sep	74.74%	2.35%	0.14%	2.34%	1.53%	0.60%	0.19%	0.86%	1.26%	15.98%	0.00%	0.00%
13-Sep	87.24%	1.39%	0.05%	2.86%	0.62%	0.64%	0.08%	1.25%	0.08%	5.79%	22.35%	0.00%
19-Sep	90.92%	2.81%	0.00%	2.37%	0.45%	0.04%	0.00%	0.40%	0.00%	3.01%	23.05%	0.00%

Fig. 12. Land use/ Land cover damage distribution from 7th to 19th of September.

The September 19, 2023, damage assessment indicates a total area coverage of 73.89% for irrigated land, 18.73% for water bodies, 2.45% for non-irrigated land, 2.29% for industrial units, and 1.93% for pasture (Fig. 12). In conclusion, the most severely impacted areas were identified as irrigated land.

Discussion

This study involved an extensive analysis of an area of central Greece (Thessaly prefecture) exposed to flood events caused by the storm Daniel on September 2023. The methodology implemented has been frequently used and provided a clear understanding of the impact assessment and flood mapping (Carreño Conde et al., 2019; Jamali and Abdul Rahman, 2019). Several studies utilized Sentinel satellite images and LULC maps to monitor and assess the damage caused by this extreme phenomenon (Billah et al., 2023; Atchyuth et al., 2023). The other part of the research utilized the FwDET tool

using the inundated areas and ALOS PALSAR DEM to calculate the floodwater depths.

The Thessaly Plain has suffered from historical floods across the years. Bathrellos et al. (2018) investigated the historical floods of the Thessaly prefecture from 1979 to 2010, where 146 flood events occurred, the most significant occurring on October 27 1980, March 23 1987, and October 22 1994. According to the Ministry of the Environment and Energy of Greece, 31.7% of the total Thessaly Plain is classified as an area of potentially high flood risk (YPEKA, 2018). Koutsoyannis and Mimikou (1996) pointed out one of the most catastrophic flood events, which occurred in October 1994, in which 80 Km of agricultural fields were damaged. Before Storm Daniel, another major storm devastated the Thessaly plain, i.e., Medicane "Ianos" (September 2020). Vassiliades et al. (2022) conducted a hydrologic/ hydraulic analysis of the event and estimated a flood extent of 234 km^2 and maximum depths of over 2 meters. After analyzing this valuable research, our study proposed a framework for rapidly mapping flood extents and floodwater depths and assessing the damage to various land uses. The first stage of the analysis focused on creating maps that illustrated the extent of the floodwater. After applying pre-processing steps to the Sentinel image, the results showed that the most significant floodwater occurred on September 10 2023, covering 516.52 km^2 showing the catastrophic effects of the phenomenon prior to Ianos (2020) where the maximum flood extent reached 253.37 km^2 (Falaras et al., 2020). These results are in agreement with other studies that imply that the maximum flood extent was reported after the end of the phenomenon (Jamali and Abdul Rahman, 2019; Tripathi et al., 2020). The proposed SAR-based inundation framework has been applied in similar events such as storms, typhoons or monsoon periods, however there are limitations of their perfomarnce in dense urban areas (Pramanick et al., 2022; Cerbelaud et al., 2021; Chung et al., 2015). Regarding the damage assessment, the most impacted LULC classes were the irrigated and non-irrigated land, which addressed more than half of the study area. Implementing the FwDET tool provided solid and valuable information about the floodwater depths. However, in our comprehensive comparison to the Copernicus monitoring products, we found that the depth values are overestimated. On September 7, 2023, the Copernicus product recorded a maximum depth of 6.49 meters, whereas another product for the same date showed higher values. On September 9, 2023, Copernicus reported water depths up to 6.00 meters, while FwDET indicated 9.94 meters. Additionally, a recent study on post-event analysis by Dimitriou (2024) reported similar floodwater depths. Peneus station recorded 8.47 m on September 8, 2023, compared to our values of 9.94 m on September 10, 2023, and 7.35 m on September 13, 2023, in northeastern Thessaly. At Nomi station in western Thessaly, the maximum depth was estimated to be around 6.42 meters on September 7, while FwDET results reached 9.49 meters in the same region on the same date. Nevertheless, different values could be interpreted due to the gap in the period of the products and monitoring stations used to compare. Initial increases were observed from September 7 to 10, 2023, followed by a gradual decline until September 19, 2023. Moreover, another research has demonstrated that FwDET is a versatile tool that can help emergency systems respond quickly by identifying critical regions that require assistance (Das et al., 2023; Sohail et al., 2023). Therefore, it is essential to construct specific types of infrastructure in vulnerable areas to minimize the damage caused by floods. These types of infrastructures include multifunctional dams for irrigation, hydropower production, flood control and domestic water supplies. Additionally, they should incorporate strategic environmental interventions such as rainwater harvesting systems and reforestation programs. However, concerns were raised regarding the drawbacks of employing FwDET, such as difficulties in acquiring high-resolution DEMs and heightened uncertainty when dealing with extensively fragmented flood extents (Cohen et al., 2019). The precision and timing of the remotely sensed flood map in relation to the flood peak are expected to constitute the primary factors contributing to uncertainty in FwDET's estimations of flood depth.

Conclusion

Thessaly Plain is well-known as one of the most disaster-affected areas on the territory of Greece regarding flood events. According to Ministry reports, the area has suffered more than 146 flood events since 1979 and is under significant risk. Large-scale environmental monitoring relies heavily on commercial and free Earth observation (EO) satellite sensor data. Due to various recent climate change phenomena and their effects on the environment, which have resulted in natural disasters such as flash floods, the use of SAR satellite sensors and modern developed tools such as the FwDET are valuable sources of information for estimating the impact and monitoring of current catastrophic events. Implementing appropriate and prompt action can significantly reduce the damage caused by these flood episodes. Notably, changes in the hydrological cycle components that could be impacted by climate change are expected to increase the frequency and occurrence of extreme floods.

Acknowledgement

This research was supported by the Slovak Research and Development Agency under Contract No. APVV 19-0340 and the VEGA Grant Agency No. VEGA 1/0782/21 and VEGA1/0577/23. The authors are grateful for the support of their research.

References

Atchyuth, B. A. S., Swain, R., Das, P. (2023): Near real-time flood inundation and hazard mapping of Baitarani River Basin using Google Earth Engine and SAR imagery. Environmental Monitoring and Assessment, 195(11), 1331.

Aziz, N. A., Alwan, I. A. (2021): An accuracy analysis comparison of supervised classification methods for

mapping land cover using sentinel 2 images in the Al-Hawizeh marsh area, southern Iraq. Geomatics and Environmental Engineering, 15(1), 5–21.

Bathrellos, G. D., Skilodimou, H. D., Soukis, K., Koskeridou, E. (2018): Temporal and spatial analysis of flood occurrences in the drainage basin of pinios river (thessaly, central greece). *Land*, *7*(3), 106.

Billah, M., Islam, A. S., Mamoon, W. B., Rahman, M. R. (2023): Random forest classifications for landuse mapping to assess rapid flood damage using Sentinel-1 and Sentinel-2 data. Remote Sensing Applications: Society and Environment, 30, 100947. https://doi.org/10.1016/ j.rsase.2023.100947

Bioresita, F., Puissant, A., Stumpf, A., Malet, J. P. (2019): Fusion of Sentinel-1 and Sentinel-2 image time series for permanent and temporary surface water mapping. International Journal of Remote Sensing, 40(23), 9026–9049.

Buta, C., Mihai, G., Stănescu, M. (2020): Flood risk assessment based on flood hazard and vulnerability indexes. Ovidius University Annals of Constanta-Series Civil Engineering, 22(1), 127–137.

Carreño Conde, F., De Mata Muñoz, M. (2019): Flood monitoring based on the study of Sentinel-1 SAR images: The Ebro River case study. Water, 11(12), 2454.

Cerbelaud, A., Roupioz, L., Blanchet, G., Breil, P., Briottet, X. (2021): A repeatable change detection approach to map extreme storm-related damages caused by intense surface runoff based on optical and SAR remote sensing: Evidence from three case studies in the South of France. ISPRS Journal of Photogrammetry and Remote Sensing, 182, 153–175. https://doi.org/10.1016/j.isprsjprs.2021. 10.013

Chung, H., Liu, C., Cheng, I., Lee, Y., Shieh, M. (2015): Rapid Response to a Typhoon-Induced Flood with an SAR-Derived Map of Inundated Areas: Case Study and Validation. Remote Sensing, 7(9), 11954–11973. https://doi.org/10.3390/rs70911954

Cohen, S., Brakenridge, G. R., Kettner, A., Bates, B., Nelson, J., McDonald, R., ..., Zhang, J. (2018): Estimating floodwater depths from flood inundation maps and topography. JAWRA Journal of the American Water Resources Association, 54(4), 847–858.

Cohen, S., Raney, A., Munasinghe, D., Loftis, J. D., Molthan, A., Bell, J., ..., Tsang, Y. P. (2019): The Floodwater Depth Estimation Tool (FwDET v2.0) for improved remote sensing analysis of coastal flooding. Natural Hazards and Earth System Sciences, 19(9), 2053–2065.

Craciunescu, V., Stancalie, G., Irimescu, A., Catana, S., Mihailescu, D., Morcov, G., Constantinescu, S. (2016): MODIS-based multi-parametric platform for mapping of flood affected areas. Case study: 2006 Danube extreme flood in Romania. Journal of Hydrology and Hydromechanics, 64(4), 329–336.

Corine Land Cover (2018): Copernicus Land Monitoring Service. Available online: https://land.copernicus.eu

Das, P., Jensen, K., De, S., Ganguly, A. R. (2023): Flood Depth Estimation Using Synthetic Aperture Radar (SAR) Imagery and Topography: A Case Study of the 2021 and 2022 Floods in Hawkesbury Valley, Australia. In IGARSS 2023-2023 IEEE International Geoscience and Remote Sensing Symposium 2402–2405.

Diakakis, M., Deligiannakis, G., Mavroulis, S. (2011): Flooding in Peloponnese, Greece: a contribution to flood hazard assessment. In: Lambrakis, N., Stournaras, G., Katsanou, K. (eds) Advances in the research of aquatic environment, vol 1. Springer, Berlin, 199–206

Diakakis, M., Mavroulis, S., Deligiannakis, G. (2012): Floods in Greece, a statistical and spatial approach. Natural hazards, 62, 485–500.

Diakakis, M., Papagiannaki, K., Fouskaris, M. (2022): The occurrence of catastrophic multiple-fatality flash floods in the Eastern Mediterranean region. Water, 15(1), 119.

Dimitriou, E., Efstratiadis, A., Zotou, I., Papadopoulos, A., Iliopoulou, T., Sakki, G. K., ..., Koutsoyiannis, D. (2024): Post-Analysis of Daniel Extreme Flood Event in Thessaly, Central Greece: Practical Lessons and the Value of State-of-the-Art Water-Monitoring Networks. Water, 16(7), 980.

ESA Sentinel Online (2019): User Guides and Technical Guides of Sentinel-1 SAR. Available online: https://sentinel.esa.int/ web/sentinel (accessed on 8 August 2019)

Falaras, T., Diakakis, M., Lagouvardos, K., Lekkas, E., Parcharidis, I. (2020): Confluence of Operational Tracking of Flood Events In Western Thessaly's Basin (Greece) In September 2020 Based on Subsequence of Optical and Radar Copernicus Satellite Imagery.

Hrušková, K., Hlaváčiková, H., (2023): Case study: Assessment of radar-based and ground precipitation data during the flood situation in May 2021 in the Upper Hron River basin in Slovakia. Acta Hydrologica Slovaca, vol. 24, no. 2, 242–253. https://doi.org/10.31577/ahs-2023-0024.02.0027

Huang, M., Jin, S. (2020): Rapid flood mapping and evaluation with a supervised classifier and change detection in Shouguang using Sentinel-1 SAR and Sentinel-2 optical data. Remote Sensing, 12(13), 2073.

Islam, M. M., Sado, K. I. M. I. T. E. R. U., Owe, M., Brubaker, K., Ritchie, J., Rango, A. (2001): Flood damage and management modelling using satellite remote sensing data with GIS: case study of Bangladesh. Iahs Publication, 455–457.

Jamali, A., Abdul Rahman, A. (2019): Flood Mapping Using Synthetic Aperture Radar: A Case Study of Ramsar Flash Flood. The International Archives of the Photogrammetry, Remote Sensing and Spatial Information Sciences, 42, 291–295.

Jonkman, S. N., Kelman, I. (2005): An analysis of the causes and circumstances of flood disaster deaths. Disasters, 29(1), 75–97.

Kellermann, P., Schöbel, A., Kundela, G., Thieken, A. H. (2015): Estimating flood damage to railway infrastructure–the case study of the March River flood in 2006 at the Austrian Northern Railway. Natural Hazards and Earth System Sciences, 15(11), 2485–2496.

Khajehei, S., Ahmadalipour, A., Shao, W., Moradkhani, H. (2020): A place-based assessment of flash flood hazard and vulnerability in the contiguous United States. Scientific Reports, 10(1), 448.

Klemas, V. (2015): Remote sensing of floods and flood-prone areas: An overview. Journal of Coastal Research, 31(4), 1005–1013.

Koutsoyiannis, D., Mimikou, M. (1996): Management and prevention of crisis situations: floods, droughts and institutional aspects. Country Paper for Greece. 3rd EURAQUA Technical Review, Rome.

Ministry of the Environment and Energy of Greece (YPEKA) (2018): Available online: http://www.ypeka.gr/Default. aspx?tabid=37& locale=en-US (accessed on 9 February 2018).

Nadal, N. C., Zapata, R. E., Pagán, I., López, R., Agudelo, J. (2010): Building damage due to riverine and coastal floods. Journal of Water Resources Planning and Management, 136(3), 327–336.

Nguyen, N. Y., Ichikawa, Y., Ishidaira, H. (2016): Estimation of inundation depth using flood extent information and

hydrodynamic simulations. *Hydrological Research Letters*, *10*(1), 39-44.

Orengo, H. A., Krahtopoulou, A., Garcia-Molsosa, A., Palaiochoritis, K., Stamati, A. (2015): Photogrammetric re-discovery of the hidden long-term landscapes of western Thessaly, central Greece. Journal of Archaeological Science, 64, 100–109.

Pekárová, P., Halmová, D., Kubeš, R., Hlavčová, K. (2003): Synthesis of meteorological and hydrological conditions leading to extreme flooding on the Hron river basin. Acta Hydrologica Slovaca, 4, 1, 2003, 131–138.

Pramanick, N., Acharyya, R., Mukherjee, S., Mukherjee, S., Pal, I., Mitra, D., Mukhopadhyay, A. (2022): SAR based flood risk analysis: A case study Kerala flood 2018. Advances in Space Research, 69(4), 1915–1929. https://doi.org/10.1016/j.asr.2021.07.003

Psomiadis, E. (2016): Flash flood area mapping utilising SENTINEL-1 radar data. In Earth resources and environmental remote sensing/GIS applications VII (Vol. 10005, 382–392). SPIE.

Schumann, G., Di Baldassarre, G., Alsdorf, D., Bates, P. D. (2010): Near real-time flood wave approximation on large rivers from space: Application to the River Po, Italy. Water Resources Research, 46(5).

Sohail, M., Muhammad, A. (2023): Assessment of the 2022 Flood Disaster In Pakistan's Lower Indus Plain Using Sar And Optical Remote Sensing. In IGARSS 2023–2023 IEEE International Geoscience and Remote Sensing Symposium, 2173–2176).

Šoltész, A., Baroková, D., Kamel, A. H. (2011): Hydraulic modelling and flood mapping for the Latorica River in GIS environment. Acta Hydrologica Slovaca, 12, 2011, 13–21.

Thomas, C., Stamataki, I., Rosselló-Geli, J. (2023): Reconstruction of the 1974 flash flood in Sóller (Mallorca) using a hydraulic 1D/2D model. Journal of Hydrology and Hydromechanics, 71(1), 49–63.

Tripathi, G., Pandey, A. C., Parida, B. R., Kumar, A. (2020): Flood inundation mapping and impact assessment using multi-temporal optical and SAR satellite data: a case study of 2017 Flood in Darbhanga district, Bihar, India. Water Resources Management, 34, 1871–1892.

Uddin, K., Matin, M. A., Meyer, F. J. (2019): Operational flood mapping using multi-temporal Sentinel-1 SAR images: A case study from Bangladesh. Remote Sensing, 11(13), 1581.

Vasiliades, L., Farsirotou, E., Psilovikos, A. (2022): An Integrated Hydrologic/Hydraulic Analysis of the Medicane "Ianos" Flood Event in Kalentzis River Basin, Greece. In Proceedings of the 7th IAHR Europe Congress, Athens, Greece 7–9).

Výleta, R., Rončák, P., Liová, A., Valent, P., Bacigál, T., Gribovszki, Z., ..., Hlavčová, K. (2023): The testing of a multivariate probabilistic framework for reservoir safety evaluation and flood risks assessment in Slovakia. A study on the Parná and Belá Rivers. Journal of Hydrology and Hydromechanics, 71(4), 449–463.

Evangelos Leivadiotis (*corresponding author, e-mail: evangelos.leivadiotis@stuba.sk)
Prof. Ing. Silvia Kohnová, PhD.
Department of Land and Water Resources Management
Faculty of Civil Engineering
Slovak University of Technology in Bratislava
Radlinskeho 11
810 05 Bratislava
Slovak Republic

Prof. Aris Psilovikos
Department of Ichthyology and Aquatic Environment
School of Agricultural Sciences
University of Thessaly
N. Ionia Magnisias, 38446
Greece